Heat accumulation in ultra-short pulsed scanning laser ablation of metals

Franziska Bauer,[1,*] Andreas Michalowski,[1] Thomas Kiedrowski,[1] and Stefan Nolte[2]

[1]*Robert Bosch GmbH, Corporate Sector Research and Advance Engineering, Postbox 30 02 40, 70442 Stuttgart, Germany*

[2]*Institute of Applied Physics, Abbe Center of Photonics, Friedrich-Schiller-Universität Jena, Max-Wien-Platz 1, 07743 Jena, Germany*

[*]*franziska.bauer@de.bosch.com*

Abstract: High average laser powers can have a serious adverse impact on the ablation quality in ultra-short pulsed laser material processing of metals. With respect to the scanning speed, a sharp transition between a smooth, reflective and an uneven, dark ablated surface is observed. Investigating the influence of the sample temperature, it is experimentally shown that this effect stems from heat accumulation. In a numerical heat flow simulation, the critical scanning speed indicating the change in ablation quality is determined in good agreement with the experimental data.

OCIS codes: (140.3390) Laser materials processing; (140.6810) Thermal effects.

References and links

1. S. Preuss, A. Demchuk, and M. Stuke, "Sub-picosecond UV laser ablation of metals," Appl. Phys., A Mater. Sci. Process. **61**(1), 33–37 (1995).
2. S. Nolte, C. Momma, H. Jacobs, A. Tünnermann, B. Chichkov, B. Wellegehausen, and H. Welling, "Ablation of metals by ultrashort laser pulses," J. Opt. Soc. Am. B **14**(10), 2716–2722 (1997).
3. J. Cheng, W. Perrie, S. Edwardson, E. Fearon, G. Dearden, and K. Watkins, "Effects of laser operating parameters on metals micromachining with ultrafast lasers," Appl. Surf. Sci. **256**(5), 1514–1520 (2009).
4. R. Gattas and E. Mazur, "Femtosecond laser micromachining in transparent materials," Nat. Photonics **2**(4), 219–225 (2008).
5. D. Bäuerle, *Laser Processing and Chemistry* (Springer, 2011), Chap. 13.
6. R. Le Harzic, N. Huot, E. Audouard, C. Jonin, P. Laporte, S. Valette, A. Fraczkiewicz, and R. Fortunier, "Comparison of heat-affected zones due to nanosecond and femtosecond laser pulses using transmission electronic microscopy," Appl. Phys. Lett. **80**(21), 3886–3888 (2002).
7. A. Y. Vorobyev and C. Guo, "Enhanced energy coupling in femtosecond laser-metal interactions at high intensities," Opt. Express **14**(26), 13113–13119 (2006).
8. S. Eaton, H. Zhang, P. Herman, F. Yoshino, L. Shah, J. Bovatsek, and A. Arai, "Heat accumulation effects in femtosecond laser-written waveguides with variable repetition rate," Opt. Express **13**(12), 4708–4716 (2005).
9. R. Weber, T. Graf, P. Berger, V. Onuseit, M. Wiedenmann, C. Freitag, and A. Feuer, "Heat accumulation during pulsed laser materials processing," Opt. Express **22**(9), 11312–11324 (2014).
10. A. Ancona, S. Döring, C. Jauregui, F. Röser, J. Limpert, S. Nolte, and A. Tünnermann, "Femtosecond and picosecond laser drilling of metals at high repetition rates and average powers," Opt. Lett. **34**(21), 3304–3306 (2009).
11. G. Raciukaitis, M. Brikas, P. Gecys, and M. Gedvilas, "Accumulation effects in laser ablation of metals with high-repetition-rate lasers," Proc. SPIE **7005**, 70052L (2008).
12. B. Neuenschwander, B. Jaeggi, M. Schmid, V. Rouffinage, and P. Martin, "Optimization of the volume ablation rate for metals at different laser-pulse durations from ps to fs," Proc. SPIE **8243**, 824307 (2012).
13. D. Thomas, C. Foulkes-Williams, P. Rumsby, and M. Gower, "Surface modifications of polymers and ceramics induced by excimer laser radiation," in *Laser Ablation of Electronic Materials*, E. Fogarassy and S. Lazare, ed. (Elsevier Science, 1992).
14. D. Young, *High Temperature Oxidation and Corrosion of Metals* (Elsevier, 2008).
15. J. Xie and A. Kar, "Laser welding of thin sheet steel with surface oxidation," Weld. J. **78**, 342–348 (1999).
16. H. Carslaw and J. Jaeger, *Conduction of Heat in Solids* (Oxford University, 1959).
17. SEW 310, *Physikalische Eigenschaften von Stählen* (Verlag Stahleisen GmbH, 1992).

1. Introduction

Laser ablation of metals using ultra-short laser pulses enables ablative processing with micrometer precision, low surface roughness and a negligible heat-affected zone [1–4]. This

#225630 - $15.00 USD Received 28 Oct 2014; revised 28 Nov 2014; accepted 23 Dec 2014; published 16 Jan 2015

is primarily due to the fact that the energy of the ultra-short pulses is deposited on such a short timescale that strong non-equilibrium conditions are generated and that the thermal diffusion length is in the same order of magnitude as the ablation depth. Therefore, a comparatively small portion of the input energy remains as heat in the ambient bulk material [5–7].

In recent years, the number of industrial applications using ultra-short laser pulses has been continuously growing. Nevertheless, the main limitation of this technology is the comparatively low ablation rate. Therefore, a speedup of the ablation process is of prime importance. This can be accomplished by using laser sources with higher average power which either generate more pulses per time, hence have an increased repetition rate, or apply higher pulse energies. In scanning laser ablation of metals, however, both options to use the higher average laser power do not only accelerate the ablation process but also come with new challenges: Depending on the scanning speed, a transition of the ablated surface quality from smooth and free of melt residuals to bumpy and presumably thermally degraded is observed. The critical scanning speed separating the two regimes is an interesting quantity for practical applications and has, to the best of our knowledge, not yet been systematically investigated.

To study the physical mechanisms responsible for this phenomenon, the dependence of the transition in ablation quality with respect to the scanning speed is explored for different sample offset temperatures to which the sample is uniformly set using a hot plate as depicted in Fig. 1. This offset temperature is found to be a crucial parameter for the transition in ablation quality. Comparing with a numerical heat flow simulation, heat accumulation [8–11] is identified to be responsible for the observed surface degradation. Our described model offers a valuable tool to predict the critical scanning speed quantitatively.

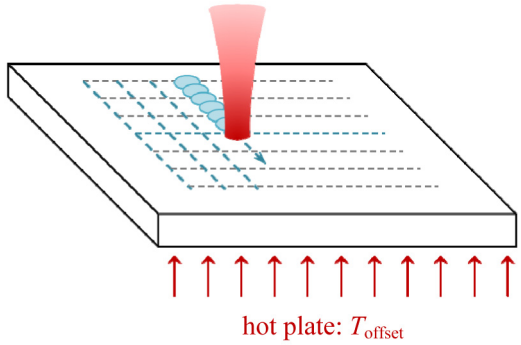

Fig. 1. Schematic of scanning laser ablation on a hot plate which uniformly sets the sample to an offset temperature.

2. Experimental setup and results

For the experiments, an Yb:YAG disk laser (Trumpf GmbH + Co.KG, TruMicro5070) with a pulse duration of about 6 ps (FWHM, sech^2 fit) at 1030 nm was used at a pulse repetition rate of 800 kHz. The circularly polarized Gaussian beam was focused on the surface of the samples to a spot size of $2w_0 = 50$ µm ($1/e^2$ diameter) with a typical peak power of 10^6 W and a typical peak intensity of 10^{15} W/m^2. Squares with a length of 1 mm were scanned with a hatch line distance of $d = 10$ µm. This overlap of 80% allows a uniformly even ablated surface. Keeping the overall energy applied for the different scanning speeds constant, the number of passes was adapted to ensure an ablation depth of about 55 µm (e.g. 60 passes at a scanning speed of $v = 3$ m/s and 120 passes at $v = 6$ m/s) which is a common depth in laser ablation applications. In the experiments, 1 mm thick samples made of stainless steel (EN Steel Number 1.4301) were machined as this material is widely used in industrial applications.

#225630 - $15.00 USD Received 28 Oct 2014; revised 28 Nov 2014; accepted 23 Dec 2014; published 16 Jan 2015

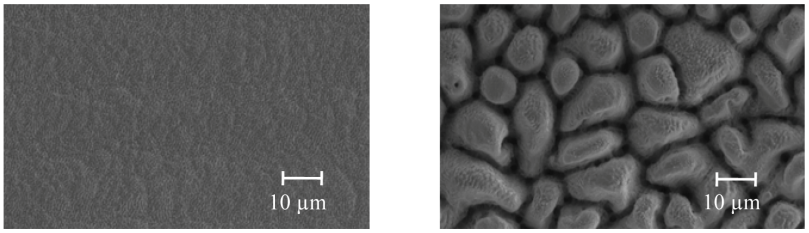

Fig. 2. SEM images of laser processed structures on stainless steel (1.4301) in the two ablation regimes ($2w_0$ = 50 µm, f_{rep} = 800 kHz, d = 10 µm, F = 0.43 J/cm^2, T_{offset} = 23 °C). (a) shows the typical smooth and reflective surface (v = 4 m/s, 80 passes). In (b) the surface is very rough and covered with small bumps (v = 0.5 m/s, 10 passes).

The polished samples (R_a<0.2 µm, S_a<0.2 µm) were placed on a hot plate whose temperature can be regulated up to T_{offset} = 315 °C. Hereby the samples may be set to a definable uniform offset temperature which is measured using a type T thermocouple (copper/constantan) attached to the sample via a kapton tape. The experiments were performed at laser fluences (pulse energy per spot area πw_0^2) of F_1 = 0.37 J/cm^2 and F_2 = 0.48 J/cm^2 which results in a high ablation efficiency [12]. For lower fluences, as we get close to the ablation threshold, the ablated surface is degraded due to cone-like structures as also observed for the ablation of polymers [13]. Higher fluences were not investigated, as the maximum scanning speed of 10 m/s (due to technical limitations of our scanning system) would not have been sufficient to cover the whole range of offset temperatures.

Depending on the processing parameters, two ablated surface quality regimes can be observed. The first regime (high-quality) is characterized by a flat surface with a roughness below R_a ~1 µm, a high reflectance and no noticeable melt depositions [Fig. 2(a)]. Usually, laser ablation of metals with ultra-short pulses is associated with the high surface quality achieved in this regime. However, the experiments also reveal the existence of a second regime (low-quality) with strongly reduced reflectance. Here, the surface is covered with bumps with a lateral size of about 10 µm [Fig. 2(b)].

A transition from the smooth to the bumpy ablated surface is found with decreasing scanning speed while all other processing parameters were kept constant. A comparison of the ablated surfaces processed at different scanning speeds is depicted in Fig. 3. From v = 0.9 m/s to 1.2 m/s the transition between the two ablation regimes is observed in this case. The minimum scanning speed still yielding a good ablation quality (less than 1% of the sample surface covered with bumps) is a characteristic parameter to describe the transition between the high-quality and the low-quality regime. We will refer to this in the following as critical scanning speed v_{crit}.

An energy dispersive x-ray spectroscopy (EDS) analysis of the laser processed surfaces shown in Fig. 2 reveals that the rough and bumpy structure has a considerably higher amount of oxygen. Figure 4(a) shows an EDS spectrum of a non-processed stainless steel surface. In Fig. 4(b), this spectrum (black) is compared to spectra of laser processed surfaces at the smooth (blue) and bumpy (red) ablation regime. The strong oxygen peak obtained in the

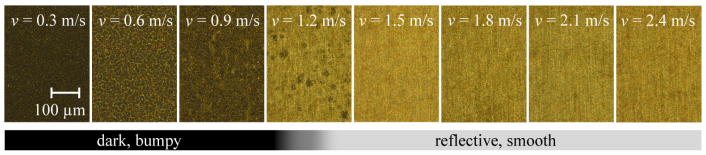

Fig. 3. Microscope images of laser processed stainless steel samples ($2w_0$ = 50 µm, f_{rep} = 800 kHz, d = 10 µm, F = 0.37 J/cm^2, T_{offset} = 23 °C). The scanning speed is varied and the number of passes is adapted to keep the total energy applied constant. Reducing the scanning speed, a sharp transition in the ablation quality from reflective and smooth to dark and bumpy is observed.

#225630 - $15.00 USD Received 28 Oct 2014; revised 28 Nov 2014; accepted 23 Dec 2014; published 16 Jan 2015

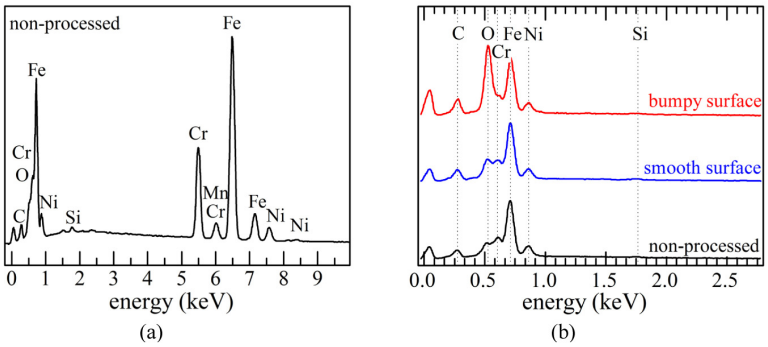

Fig. 4. In (a) an overview EDS spectrum of the unprocessed stainless steel (1.4301) sample is shown. In (b) the comparison of spectra taken on the different surfaces (normalized to the Fe peak) illustrates the considerably higher amount of oxides present on the bumpy surface.

bumpy regime proves the effect of surface oxidation. As the oxidation of metals is a temperature sensitive effect [14], the larger amount of oxides on the bumpy laser structure suggests that the surface modification is caused by high temperatures during processing. Therefore, the decreased reflectance observed for the low-quality regime is probably caused by two effects: multiple reflections induced by the bumps and a reduced reflectivity of the oxidized surface [15].

By investigating the influence of the uniform offset temperature to which the sample is set by the hot plate on v_{crit}, it is hereinafter experimentally shown that the transition from the smooth high-quality to the bumpy low-quality regime is determined by the temperature of the sample surface at the impact area of the following laser pulse. Moreover, this hypothesis is confirmed by a heat flow simulation discussed in section 3 which shows excellent agreement with the experimental data.

Figure 5 shows experimental data for the critical scanning speed v_{crit} at different sample offset temperatures T_{offset} exemplarily for two laser fluences. It is obvious that v_{crit} increases significantly with the sample offset temperature. Also, a higher fluence requires a greater scanning speed to achieve a smooth, high-quality ablation result. While the critical scanning speeds at T_{offset} = 50 °C are found to be v_{crit} = 1.9 m/s and 2.7 m/s, a sample temperature of T_{offset} = 315 °C demands scanning speeds of at least v_{crit} = 6.7 m/s and 9.9 m/s for the fluences F_1 = 0.37 J/cm^2 and F_2 = 0.48 J/cm^2, respectively. Therefore, it can be assumed that the transition between the ablation regimes is determined by a temperature threshold T_{th} locally exceeded during processing.

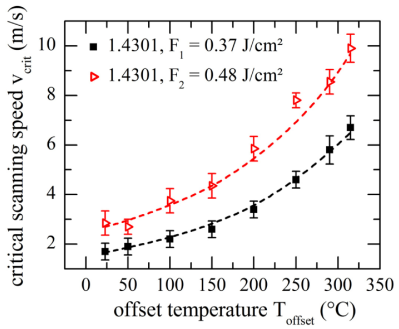

Fig. 5. Experimental data representing the rise in critical scanning speed v_{crit} when the offset temperature T_{offset} of the stainless steel sample is increased using a hot plate. A higher fluence also results in a higher critical scanning speed v_{crit} for a given offset temperature. The dashed lines show the simulated values (see Sect. 3.3) for the critical scanning speed. For the simulation, a critical saturation temperature of T_{th} = 607 °C was applied.

#225630 - $15.00 USD Received 28 Oct 2014; revised 28 Nov 2014; accepted 23 Dec 2014; published 16 Jan 2015

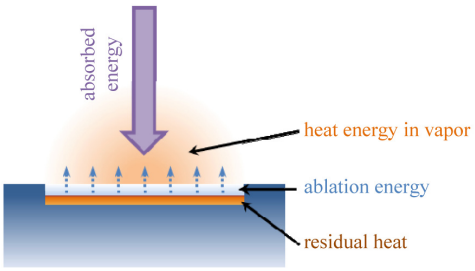

Fig. 6. Schematic illustration of the energy distribution after irradiation with an ultra-short laser pulse.

3. Model and simulation of heat accumulation

The laser pulse energy E_p incident on the sample surface is split into different parts: A certain amount is reflected and the remaining absorbed portion $\eta_{abs} \cdot E_p$ is subdivided into the ablation energy E_{abl} required to evaporate the material, the kinetic and thermal energy E_v in the vapor, and the residual heat $E_{res.heat} = \eta_{res} \cdot E_p$, as given in Eq. (1) and schematically illustrated in Fig. 6. This latter thermal energy is left locally concentrated in the surrounding of the ablation area.

$$\eta_{abs} \cdot E_p = E_{abl} + E_v + \underbrace{E_{res.heat}}_{E_{res.heat} = \eta_{res} \cdot E_p} \tag{1}$$

In order to determine the residual heat, a calorimetric setup has been used. Therefore, a thermally insulated sample has been processed using the same experimental conditions as described above and the amount of residual heat was calculated from the temperature rise of the bulk material after thermalization. The residual heat was 40% of the total laser pulse energy for $F_1 = 0.37$ J/cm^2 and 38% for $F_2 = 0.48$ J/cm^2, respectively.

For multi-pulse processing, the small amount of residual heat which is left in the material after a first laser pulse may not be completely dissipated into the sample by heat conduction before the next pulse is applied if the repetition rate is high enough. Thus, the following pulse impinges on a locally preheated workpiece and heats it up to an even higher temperature [9]. This phenomenon is strongly influenced by material properties (thermal diffusivity, reflectivity) and processing parameters (laser fluence, temporal and spatial displacement).

The effect of heat accumulation can be described quantitatively by a simple model. At the beginning, the temperature is set to the offset temperature T_{offset}. The temperature rise due to the residual heat associated with each pulse is assumed to be instantaneous as the pulse duration is orders of magnitude smaller than the timescales relevant for heat conduction. Radiative cooling is not considered within this model because for steel, heat conduction into the bulk dominates the energy loss of the surface by far.

3.1 Analytical calculation

For the calculation of the residual heat, the heat dissipation after the laser pulse is determined by the heat conduction equation. For an instantaneous point source of energy Q, the solution for the temperature rise inside an infinite homogeneous solid is given by

$$T(R,t) = \frac{Q}{\rho c\,(4\pi\kappa t)^{3/2}} \cdot e^{-\frac{R^2}{4\kappa t}} \tag{2}$$

where R denotes the distance from the point source, t the time elapsed after the instantaneous heating pulse, c the material specific heat capacity, ρ the density and κ the thermal diffusivity [16]. From this equation, the solution for an arbitrarily shaped heat source can be derived by integrating over the respective point sources described by Eq. (2):

#225630 - $15.00 USD Received 28 Oct 2014; revised 28 Nov 2014; accepted 23 Dec 2014; published 16 Jan 2015

$$T(x,y,z,t) = \int_{-\infty}^{\infty}\int_{-\infty}^{\infty}\int_{-\infty}^{\infty} \mathrm{d}x_0\ \mathrm{d}y_0\ \mathrm{d}z_0\ \frac{\tilde{Q}(x_0,y_0,z_0)}{\rho c\,(4\pi\kappa t)^{3/2}} \cdot e^{-\frac{(x-x_0)^2+(y-y_0)^2+(z-z_0)^2}{4\kappa t}} \tag{3}$$

Assuming a Gaussian surface heat source with the radius w_0 of the laser spot and a semi-infinite solid, $\tilde{Q}\ (x_0, y_0, z_0)$ is given by

$$\tilde{Q}(x_0,y_0,z_0) = \frac{4E_{\mathrm{res}}}{\pi \mathrm{w}_0^2} e^{\frac{2\cdot\left((x-x_0)^2+(y-y_0)^2\right)}{\mathrm{w}_0^2}} \cdot \delta(z-z_0). \tag{4}$$

Hence, the solution for a spatially Gaussian-shaped single pulse surface heat source can be calculated to

$$T^{\mathrm{s.p.}}_{(x_\mathrm{c},y_\mathrm{c})}(x,y,z,t) = \frac{2E_{\mathrm{res}}}{\pi\rho c\sqrt{\pi\kappa t}\,(8\kappa t + w_0^2)} \cdot e^{\frac{(x-x_\mathrm{c})^2+(y-y_\mathrm{c})^2}{4\kappa t}\left(\frac{w_0^2}{8\kappa t+w_0^2}-1\right)} \cdot e^{-\frac{z^2}{4\kappa t}} \tag{5}$$

where $(x - x_\mathrm{c})$, $(y - y_\mathrm{c})$ and z represent the respective distances from the centre $(x_\mathrm{c}, y_\mathrm{c}, 0)$ of the Gaussian distribution.

A new pulse is applied after $\Delta t_{p\text{-}p} = 1/f_{\mathrm{rep}}$ and is hence superposed onto the temperature distribution of the previous pulse. Also, the spatial displacement $v\Delta t_{p\text{-}p}$ of the subsequent pulses resulting from the scanning speed v is accounted for by adjusting the centre coordinates of the Gaussian distribution. The temperature distribution after N pulses is thus given by

$$T(x,y,z,t) = \sum_{i=0}^{N} T^{\mathrm{s.p.}}_{(x_{c_i},y_{c_i})}(x,y,z,t+i\cdot\Delta t_{p-p}) \tag{6}$$

where $x_{c_i} = i \cdot v\Delta t_{p\text{-}p}$ for scanning in x-direction and starting at the origin.

This analytical calculation already represents a valuable tool to estimate the heat accumulation in scanning ultra-short pulsed laser ablation. For a closer examination, however, the temperature dependent thermophysical properties of the sample need to be taken into consideration which requires a numerical method.

3.2 Numerical model

In this finite difference model, the temperature of all elements is initially set to the sample offset temperature $T(i\cdot\Delta x, j\cdot\Delta y, k\cdot\Delta z, t_0 = 0) = T_{\mathrm{offset}}$ (for all i, j, k). If a pulse is applied in between the time steps $(n - 1)$ and n, the energy of the respective surface elements is increased according to

$$E(x_i,y_j,z_0,t_n) = E(x_i,y_j,z_0,t_{n-1}) + E_{\mathrm{res}}\,\Delta x\,\Delta y \cdot \exp\left\{-\frac{2}{w_0^2}\cdot[(x_i-x_\mathrm{c})^2+(y_j-y_\mathrm{c})^2]\right\}. \tag{7}$$

Thus, the heat is deposited only in the surface layer of the mesh. This is justified as the thermal diffusion length of ultra-short laser pulses is orders of magnitude shorter than the discretization step $\Delta z = 0.5$ µm. The resulting temperature rise can then be calculated to give

$$T(x_i,y_j,z_k,t_n) = \frac{E(x_i,y_j,z_k,t_n)}{c\,\rho\,\Delta x\,\Delta y\,\Delta z} \tag{8}$$

The heat exchange of adjacent elements within one time step according to the heat conduction equation can be described using a discrete convolution (Eq. (9a)), where the (3 × 3 × 3) convolution matrix B is given by Eq. (9b).

#225630 - $15.00 USD Received 28 Oct 2014; revised 28 Nov 2014; accepted 23 Dec 2014; published 16 Jan 2015

$$T(\vec{x},t_n) = (B * T)(\vec{x},t_{n-1}) \tag{9a}$$

$$B_{1jk} = B_{3jk} = \frac{\kappa\Delta t}{(\Delta x)^2}\delta_{22},\ B_2 = \begin{pmatrix} 0 & \frac{\kappa\Delta t}{(\Delta z)^2} & 0 \\ \frac{\kappa\Delta t}{(\Delta y)^2} & 1-\frac{2\kappa\Delta t}{(\Delta x)^2+(\Delta y)^2+(\Delta z)^2} & \frac{\kappa\Delta t}{(\Delta y)^2} \\ 0 & \frac{\kappa\Delta t}{(\Delta z)^2} & 0 \end{pmatrix} \tag{9b}$$

Again, the subsequent pulses are superposed taking into account the temporal and spatial displacement determined by the repetition rate and the scanning speed. The temporal resolution was chosen to be Δt = 1 ns. For the numerical model, the temperature dependent thermophysical properties of stainless steel (1.4301) are interpolated from the data given in Table 1. The corresponding density is ρ = 7920 kg/m^3 [17].

For all temperatures higher than 800 °C, it is a reasonable approximation to use the values for 800 °C. From Eq. (5), it can be easily seen that for short times $t << w_0^2/8\kappa$, the surface temperature (z = 0) at the center coordinates $x = x_c$, $y = y_c$ is given by

$$T^{\text{s.p.}}_{(x_c,y_c)}(t) \approx \frac{2E_{\text{res}}}{\pi\rho c\sqrt{\pi\kappa t}\,w_0^2}. \tag{10}$$

Thus, for the typical processing parameters applied (F = 0.37 J/cm^2, η_{res} = 0.4), the temperature decays to 800 °C after less than 40 ns. As this time is much shorter than the time between two subsequent pulses, the use of the values for 800 °C also for higher temperatures will only result in minor errors.

Table 1. Thermophysical Properties of 1.4301 Stainless Steel[a]

T (°C)	κ (10^{-6} m^2/s)	c (J/kgK)
−100	3.7	440
0	3.8	468
20	3.9	472
100	4.3	487
200	4.3	503
300	4.6	512
400	4.7	520
500	4.9	530
600	5.0	541
700	5.3	551
800	5.7	559

[a]From SEW 310, *Physikalische Eigenschaften von Stählen* (Verlag Stahleisen GmbH, 1992).

3.3 Saturation temperature simulation based on numerical model

In Fig. 7(a), the maximum temperature value at the surface is plotted as a function of time for the first 20 pulses and a lateral pulse distance of 5 µm which corresponds to 10% of the spot diameter. Each pulse leads to an instantaneous temperature rise followed by a decay caused by heat conduction. Initially, the deposited heat does not fully dissipate before the next pulse. After approximately 10 pulses, a steady-state regime is obtained. Figure 7(b) shows temperature profiles over depth at the coordinates of maximum temperature directly before the second (solid) and the tenth (dashed) pulse are applied, respectively. The saturation behavior in Fig. 7(a) is an implication of the stronger temperature gradient associated with a larger heat flow rate. Considering the lower envelope of the temperature values reached directly before the subsequent pulse is applied in Fig. 7(a), a saturation value T_{sat} can be defined.

#225630 - $15.00 USD Received 28 Oct 2014; revised 28 Nov 2014; accepted 23 Dec 2014; published 16 Jan 2015

In the experiments, the smooth ablation quality was only achieved for scanning speeds $v > v_{crit}$. As it has been shown that the transition in ablation quality depends on the sample offset temperature, it is assumed that there exists a certain threshold temperature T_{th} causing the change in ablation quality when exceeded. Figure 8 shows the simulated temperatures for scanning speeds above and below the critical value of v_{crit} = 4.6 m/s, valid for the laser parameters used and T_{offset} = 250 °C. A smaller scanning speed leads to a higher saturation temperature T_{sat} and vice versa. In the simulation, the boundary between the ablation regimes

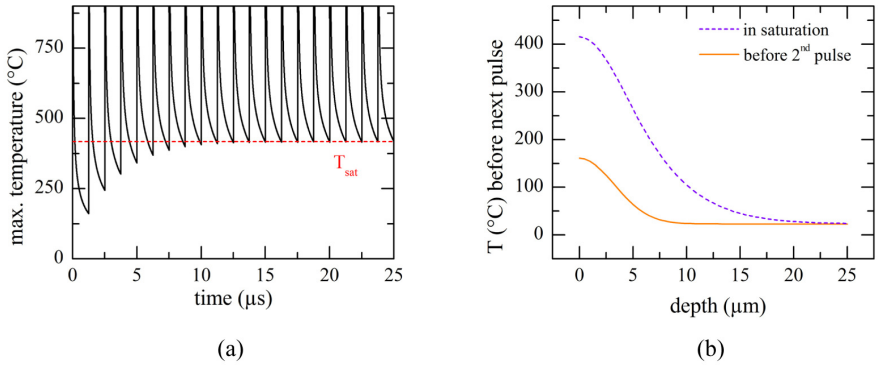

Fig. 7. (a) Simulation of heat accumulation using f_{rep} = 800 kHz, $2w_0$ = 50 µm, F_1 = 0.37 J/cm^2, T_{offset} = 23 °C, v = 4 m/s, η_{res} = 0.4, material parameters for 1.4301 stainless steel according to Table 1. The maximum temperature at the surface is plotted against time. After ~10 pulses, a saturation temperature T_{sat} is reached. In (b) the temperature directly before the next pulse at the position of maximum temperature is plotted against depth z. The temperature gradient in saturation is much greater than in the beginning and allows a more efficient heat conduction.

is determined by $T_{th} = T_{sat}(v_{crit})$. Parameters yielding $T_{sat} \leq T_{th}$ represent the smooth, reflective ablation surface, whereas with $T_{sat} > T_{th}$, the surface is degraded due to thermal effects.

In Fig. 5, a comparison of simulation results and the experimental values for the critical scanning speed v_{crit} at different sample offset temperatures T_{offset} is depicted. Using a critical saturation temperature of T_{th} = 607 °C and determining the scanning speed for each offset temperature T_{offset} such that $T_{sat} = T_{th}$ is reached, a good agreement with the experimental data is observed for both laser fluences. From the curve fitting, the uncertainty of T_{th} is found to be about ± 10 °C. The exact physical meaning of this threshold temperature T_{th} is to be investigated in future work. According to Eq. (8), a higher fluence leads to a greater temperature rise and hence requires a higher scanning speed to reach $T_{sat} = T_{th}$. This experimentally observed increase of v_{crit} from F_1 to F_2 for a fixed T_{offset} is also well reflected by the simulation. Therefore, for a given critical saturation temperature, the explained model allows describing the transition from the smooth to the bumpy ablation regime quantitatively for different fluences.

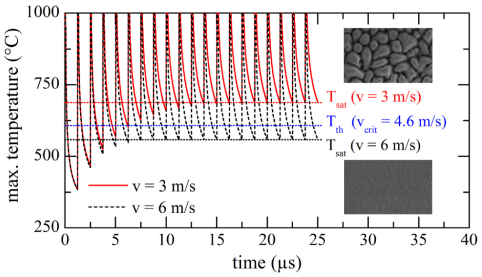

Fig. 8. Maximum temperature value plotted as a function of time for a fluence of 0.37 J/cm^2, a spot diameter of 50 µm, a repetition rate of 800 kHz and different scanning speeds. In contrast to the simulation shown in Fig. 7, the sample offset temperature was chosen to be T_{offset} = 250 °C.

#225630 - $15.00 USD Received 28 Oct 2014; revised 28 Nov 2014; accepted 23 Dec 2014; published 16 Jan 2015

4. Summary and conclusion

In the scope of this study, it is shown that in scanning ultra-short pulse laser processing of metals, there exist two ablation regimes differing significantly in ablation quality: in the high-quality regime, the ablated surface is smooth and reflective; the surface in the low-quality regime, however, has a much lower reflectance, is oxidized and covered with small bumps of about 10 µm. A transition from the bumpy to the smooth ablation regime is accomplished by increasing the scanning speed. The minimum scanning speed v_{crit} yielding a high-quality ablated surface was identified as an important parameter. It increases for higher fluences and sample offset temperatures. Considering the temperature rise due to the deposited heat remaining in the laser-irradiated area after each pulse and taking into account the temporal and spatial displacement of the subsequent pulses, a heat flow model for scanning ultra-short pulse laser machining was developed. From the model it can be deduced that heat accumulation leads to a saturation state of the surface temperature depending on the processing parameters. Assuming a threshold temperature of T_{th} = 607 °C determining the change in ablation quality of the investigated stainless steel (1.4301), the critical scanning speed can hereby be simulated and agrees well with the experimental data.

#225630 - $15.00 USD Received 28 Oct 2014; revised 28 Nov 2014; accepted 23 Dec 2014; published 16 Jan 2015